First Observation of Synchrotron Radiation Spikes for Transverse Electron Beam Size Measurements at a Free-Electron Laser

Andrei Trebushinin,[*,†] Svitozar Serkez,[†] Wolfgang Freund, Andreas Koch, Jan Grünert, and Gianluca Geloni
European XFEL GmbH, Holzkoppel 4, 22869 Schenefeld, Germany

Weilun Qin[‡,§] and Sergey Tomin
Deutsches Elektronen-Synchrotron, Notkestraße 85, 22607 Hamburg, Germany

(Received 14 May 2025; accepted 2 September 2025; published 20 November 2025)

We report the observation of transverse intensity fluctuations—spikes—in synchrotron radiation from a single undulator cell at the European XFEL after monochromatization. Autocorrelation analysis of the recorded events confirms that these fluctuations originate from the partial transverse coherence of the radiation. By calculating the second-order autocorrelation function, we determined the averaged transverse slice size of the electron beam along the SASE1 undulator. The measurements were performed with 5.49 keV x-ray photons using a commissioning silicon monochromator with (111) Bragg reflection and an x-ray imager. This technique enables undulator cell-by-cell diagnostics of the transverse electron beam size at free-electron laser facilities.

DOI: 10.1103/z89g-f7j6

Stochastic radiation sources produce randomly fluctuating field distributions, with fluctuation scales set by coherence length and time. However, the direct observation of these fluctuations is often challenging. For example, the extremely short coherence time of broadband visible thermal radiation makes direct detection of these field fluctuations virtually impossible. Even for well-studied sources like sunlight, coherence properties remain not completely explored [1], with significant advances only recently achieved, such as for example the first direct measurement of sunlight spatial coherence [2]. These studies emphasize the difficulty of characterizing stochastic radiation, even for ubiquitous sources.

A particularly notable case of stochastic radiation is found in free-electron lasers (FELs), where self-amplified spontaneous emission (SASE) exhibits thermal-source-like behavior in the linear regime of FEL operation [3,4]. SASE radiation is characterized by stochastic "spikes" originating from shot noise in the electron beam [4–6]. However, due to the transverse mode selection mechanism during the FEL process, these spikes are only associated to the time-frequency domain. These spikes are routinely observed with spectrometers of SASE FEL facilities, for example [7,8], as well as simulated numerically [9].

Fundamentally, SASE originates from synchrotron radiation and inherits its statistical properties while undergoing amplification and bandwidth narrowing. Synchrotron radiation, despite its apparent "stability," also exhibits fluctuating fields, both temporally and transversely across the radiation pulse. In storage rings, the longer electron bunches—compared to those in linear accelerators—make the direct measurement of intensity fluctuations particularly challenging, requiring high-resolution monochromators [10,11]. However, at linear accelerators, the bunch duration is shorter by an order of magnitude, so one may expect to observe fluctuating field distributions (spikes) in synchrotron radiation in the transverse domain, even when using conventional monochromators.

Typically, the coherence time of radiation from a single electron and its transverse virtual source size are smaller than the corresponding electron beam dimensions. In this case, synchrotron radiation at its source—the undulator—effectively imprints the six-dimensional phase-space distribution of the electron beam to the synchrotron radiation. The transformation of the coherence properties between Fourier domains are governed by the generalized Wiener-Khinchin theorem [12,13] for quasistationary sources in the longitudinal domain and by the generalized [14,15] Van Cittert–Zernike theorem [16,17] in the transverse domain. So, these field fluctuations—spikes—encode information about the electron beam transverse size and duration

[*]Contact author: andrei.trebushinin@xfel.eu
[†]These authors contributed equally to this work.
[‡]Present address: Institute of High Energy Physics, Chinese Academy of Sciences, Beijing 100049, China.
[§]Present address: Spallation Neutron Source Science Center, Dongguan 523803, China.

following these theorems. Namely this was used in the iconical experiment [18,19] and then widely applied in various areas of research [20–23] including FEL physics [24–26] but for the longitudinal domain. Consequently, measuring the transverse coherence length or spectral coherence length allows one to infer the beam size or duration, respectively.

Many works were dedicated to measuring the transverse profile of the electron beam at storage rings [27,28] using the correlation analysis, for example [10], and related techniques [29–31]. Notably, in pioneering work at the Spring-8 facility authors resolved the spectral spikes using a monochromator with 5.5 meV bandwidth at 14.41 keV [11] photon energy and so measured the electron beam duration. With this setup the authors also measured the transverse coherence length [10], which was used to determine the electron beam size. However, direct noninterferometric observation of transverse spikes in synchrotron radiation on a shot-to-shot basis has remained elusive to the best of our knowledge.

In this Letter, we present a direct observation of the spatial distribution of monochromatized synchrotron radiation, which exhibits, shot to shot, visually discernible spike structures. To confirm this observation, we proceed with a noninterferometric autocorrelation analysis of the detected events. This analysis enables us to verify the typical transverse spike distribution, with the width corresponding to the transverse coherence length of the radiation. Using this information, we retrieved the electron beam transverse size based on the generalized Van Cittert–Zernike theorem.

Moreover, this method makes it possible to differentiate between two types of beam sizes in the presence of spatiotemporal tilts: the averaged transverse size of slices along the electron beam (hereafter referred to as the "averaged transverse slice size") can be measured using a monochromator with a bandwidth broader than a single spectral spike, while narrowing the bandwidth down to a single spike and less yields the *projected* transverse size. By contrast, wire scanners—commonly used at FEL facilities to measure the electron beam [32,33] size—can only measure the projected size. We study this effect in detail in our companion paper [34].

The results reported in this Letter highlight the potential of this method for diagnosing the averaged transverse slice size of the electron beam on a cell-by-cell basis along SASE undulators for advancing FEL performance. This capability is particularly critical for advanced schemes such as self-seeding [35–45], two-color generation [46–50], and ultrashort pulse generation [26,50–57] at sub-fs levels, especially in scenarios involving complex electron beam phase-space configurations such as tilted [50] or chirped beams [25]. At the same time, in this Letter we directly demonstrate that synchrotron radiation exhibits spiky intensity distributions, as described in [58,59], which are of academic interest.

We conducted the experiment at the SASE1 undulator of the European XFEL facility using the existing beamline devices: the commissioning silicon monochromator (K-mono) [60] and the synchrotron radiation imager (SR imager) [61]. These measurements did not require any specific configuration or modification to the hardware. The experimental setup is shown in Fig. 1. In the experiment, we used the Si (111) reflection for the K-mono, providing a relative spectral resolution of $\Delta E_{T_\omega}/E_{T_\omega} = 2 \times 10^{-4}$ [60] at full width at half maximum (FWHM). For the SR imager, we utilized a yttrium-aluminum garnet (YAG) screen. Although it is an order of magnitude less sensitive, 0.54 lsb/ph (least significant bit per photon) compared to the gadolinium oxysulfide screen (6.3 lsb/ph), the YAG screen offers 2 times better spatial resolution, achieving 30 μm (FWHM).

As Fig. 1 illustrates, a monochromator transmits only a few spectral spikes, which amount to

$$\frac{1}{M_L} = \frac{\hbar}{\sqrt{2}\Delta E_{T_\omega}\sigma_T}, \tag{1}$$

where ΔE_{T_ω} is the monochromator bandwidth, σ_T is the electron beam duration (both measures are given in standard deviation), and $\hbar$ is the reduced Planck constant.

The resulting image at the SR imager consists of a distribution averaged over M_L longitudinal spikes. Such averaging leads to a reduction in the contrast of the intensity distribution, as shown in Fig. 1, quantitatively manifested as a decrease in the maximum value of the correlation function by this factor M_L,

$$\frac{\langle I_1 I_2\rangle}{\langle I_1\rangle\langle I_2\rangle} \approx 1 + \frac{\hbar}{\sqrt{2}\Delta E_{T_\omega}\sigma_T}|g^{(1)}(z, \Delta\vec{r}, \vec{\bar{r}}, \bar{\omega}_0)|^2. \tag{2}$$

For brevity, $I_{1,2}$ denotes a pair of intensity values at points separated by $|\Delta\vec{r}|$, and $\bar{\omega}$ is the central frequency of the radiation within the monochromator bandwidth E_{T_ω}. The variable $\Delta\vec{r}$ is defined as $\Delta\vec{r} = \vec{r}_2 - \vec{r}_1$, and $\vec{\bar{r}} = (\vec{r}_1 + \vec{r}_2)/2$, where $\vec{r}_{1,2}$ denote the transverse positions. $g^{(1)}(z, \Delta\vec{r}, \bar{\omega}_0)$ is the cross-spectral density function at the detector position.

To estimate M_L, we measured the duration of the electron beam using noninvasive THz spectroscopy for bunch current profile reconstruction at the European XFEL [62]. This corresponds to the SR pulse duration and is equal to $\delta\tau = 37 \pm 3$ fs (FWHM). Using Eq. (1), we estimated that there are $M_L = 16 \pm 2$ longitudinal spikes. This result demonstrates the feasibility of extracting a reasonably small number of spikes within the bandwidth of a conventional monochromator, made possible thanks to the short electron bunches delivered by a linear accelerator.

In practice, the resulting distribution at the detector is significantly affected by the detector shot noise and, to our experience, detecting radiation from passage of only one

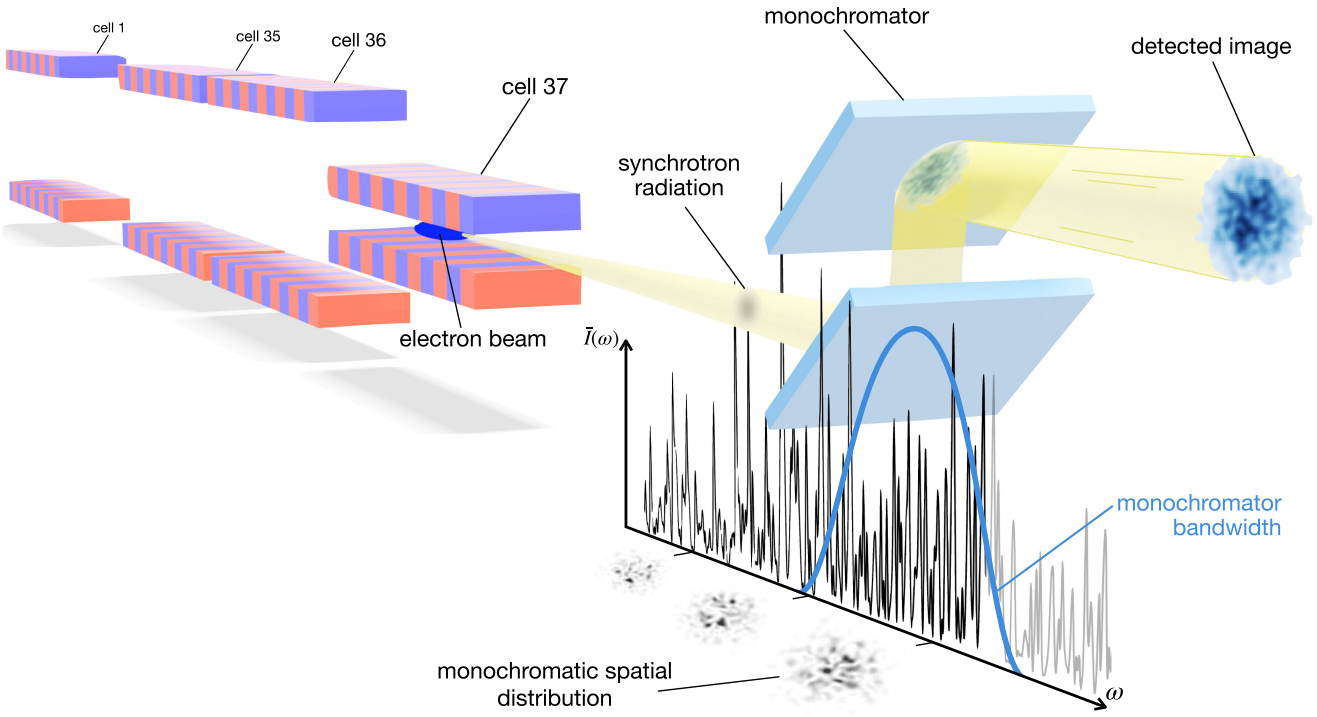

FIG. 1. A schematic representation of the experimental setup is shown. Radiation is emitted from cell 37 at SASE1. The blue distribution, located after the monochromator, represents a simulation of the averaged transverse distribution from different longitudinal spikes following monochromatization. The black-and-white spatial distribution near the spectrum illustrates the monochromatic intensity distribution from the various spikes.

electron bunch per 10 Hz train is not enough to see the signal. To ensure acceptable photon flux levels at the SR imager, we recorded radiation from several successive electron bunches per 10 Hz train per one recorded event. This approach is justified, as explained before, by the fact that the spikes are statistically independent, making this averaging equivalent to averaging over $M_L = 16 \pm 2$ spikes *multiplied* by the number of electron bunches ($N_e = 13$). Such averaging results in a corresponding drop in the maximum value of cross-spectral density function in Eq. (2) by a factor of $M_L N_e$.

We present the typical signal observed on the SR imager from a 5.49 keV photon beam in Fig. 2(a). For comparison, the result of a simulation based on the algorithm described in [59] is shown in Fig. 2(b). Essential aspects of the simulation, as well as the numerical reproduction of the experimental results, are discussed in detail in [34]. An animated version of Fig. 2(a), showing the recorded events, is provided in Supplemental Material (SM) [63]; one can observe event-to-event variations with features comparable in size to the correlation function [depicted for reference in the upper left corner in Fig. 2(a)]. To the best of our knowledge, this is the first direct observation of synchrotron radiation spikes in the transverse domain.

We then performed an autocorrelation analysis of the ensemble of recorded events to confirm that the features observed in Fig. 2 are statistically significant and originate from the coherence properties of the radiation. Prior to performing the correlation analysis, we subtracted the signal bias, calculated from dark images as the mean value for each pixel. The detector counts K include both the signal counts I and the detector noise N: $K = I + N$. Therefore, by autocorrelating the detected counts, we obtain

$$\frac{\langle K_1 K_2 \rangle}{\langle K_1 \rangle \langle K_2 \rangle} = \frac{\langle I_1 I_2 \rangle}{\langle I_1 \rangle \langle I_2 \rangle} + \frac{\langle N_1 N_2 \rangle}{\langle I_1 \rangle \langle I_2 \rangle}, \tag{3}$$

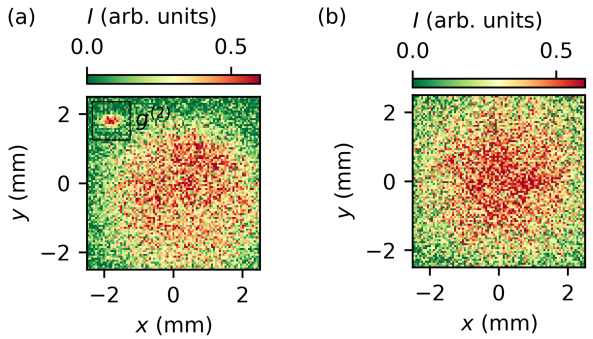

FIG. 2. Single event detected in the experiment is shown in (a), and the corresponding simulated signal is presented in (b). Spiky features can be distinguished by comparing their size with respect to the measured correlation function shown in the upper-left corner of (a).

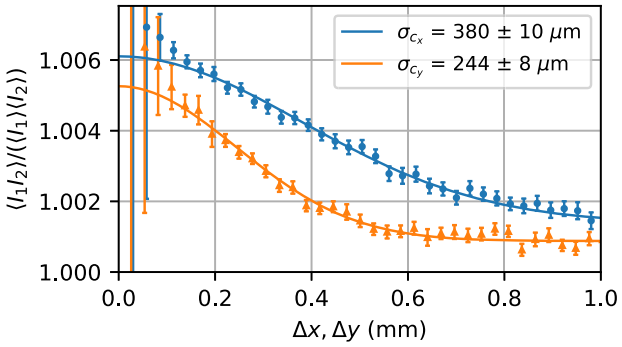

FIG. 3. Measured $g^{(2)}$ function for both horizontal and vertical directions, presented with blue dots (x) and orange triangles (y), respectively, along with their fitting results represented by the solid lines of the corresponding color.

where $N_{1,2}$ are noise counts, which cannot be directly determined from the signal data. In order to recover the actual signal autocorrelation $\langle I_1 I_2\rangle/\langle I_1\rangle\langle I_2\rangle$, we used "dark" images and calculated the noise correlation, which we normalized by the signal intensities. We assumed that detector noise statistical properties did not change during the experiment. Additionally, we suppose there is no correlation between the photon counts and noise counts, such that $\langle I_{1,2} N_{2,1}\rangle = 0$. This assumption is justified by the very low useful signal level, which we believe could not induce crosstalk between detector pixels.

As we mentioned, during the experiment we encountered signal-to-noise ratios around unity or lower. To mitigate the impact of noise, we leveraged the fact that synchrotron radiation is quasihomogeneous in the sense of statistical optics [64], meaning that $g^{(1)}(z, \Delta\vec{r}, \vec{\bar{r}}, \bar{\omega}_0)$ does not depend on $\vec{\bar{r}}$, and we averaged the correlation over the $\vec{\bar{r}}$ variable. This averaging suppressed the influence of noise on the correlation function effectively increasing collected statistics. The same averaging was done for noise autocorrelation. We present the detail on this procedure in [34].

Then by subtracting the noise correlation level we obtain the signal autocorrelation $\langle I_1 I_2\rangle/\langle I_1\rangle\langle I_2\rangle$, presented in Fig. 3.

The presented uncertainties are challenging to express in the usual form, typically used for coincidence circuits, where exact true and false actions of the detector are known. In our case, we could not separate these two types of counts. Instead, we calculated the standard deviation across the initially measured correlations over the detector area, as described in Eq. (4),

$$\delta_K = \left(\sigma\left(\frac{\langle K_1 K_2\rangle}{\langle K_1\rangle\langle K_2\rangle}\right)^2 + \sigma\left(\frac{\langle N_1 N_2\rangle}{\langle I_1\rangle\langle I_2\rangle}\right)^2 + \sigma\left(\frac{1}{\sqrt{B}}\sigma\left(\frac{\langle K_1 K_2\rangle_b}{\langle K_1\rangle_b\langle K_2\rangle_b}\right)\right)^2\right)^{1/2}. \quad (4)$$

Additionally, we accounted for variations in the signal standard deviation by batching the data into smaller ensembles to capture any temporal variations. A more detailed discussion on uncertainty estimations is provided in [34].

Here, the subscript b in $\langle\ldots\rangle_b$ denotes ensemble averaging over random subsets sampled from the initially recorded ensemble, B represents the size ratio between the initial ensemble and the subset, and $\sigma(\cdot)$ denotes the standard deviation operation.

The cross-spectral function is related to the intensity distribution of a radiation source via a Fourier transform, as described by the generalized Van Cittert–Zernike theorem [15–17]. Then, the electron beam width is connected to the width of the distribution shown in Fig. 3 through the following relationship [58]:

$$\sigma_{x,y} = \frac{z\lambda}{2\sqrt{2}\pi\sigma_{c_x,c_y}}, \quad (5)$$

where σ_{c_x,c_y} is the width of $|g^{(1)}|^2$ under the assumption that it follows a Gaussian distribution. This equation can be derived from Eq. (92) in [58]. The data was fitted using the least mean square method, applying a Gaussian distribution plus bias. From this fit, we retrieved the standard deviation (σ_{c_x,c_y}) of the distribution, with the uncertainties arising from the fitting process. For the specific measurement presented in Fig. 3 (for cell 25 along SASE1), we determined the electron beam transverse size to be $\sigma_x = 16.8 \pm 0.4$ μm and $\sigma_y = 26 \pm 0.3$ μm.

The maximum values of the measured correlation functions are 0.0048(2) for the x dimension and 0.0044(2) for the y dimension, both obtained from curve fitting. These values closely agree with the estimation based on the number of spikes falling within the K-mono bandwidth, averaged over the number of electron bunches,

$$\frac{1}{M_L N_e} = \frac{1}{(16 \pm 2) \times 13} = 0.0049(6). \quad (6)$$

To confirm that the measured autocorrelation function distributions are indeed related to the electron beam size, we intentionally varied it. This was done by adjusting the magnetic field strength of one of the quadrupoles located upstream of the SASE1 undulator lattice. Such an adjustment is expected to introduce a sinusoidal variation in the electron beam size along the undulator, effectively creating a mismatch with respect to the nominal conditions, in which the transverse size of the electron beam remains nearly constant along SASE1. Successive measurements were performed under this magnetic lattice configuration, starting from the last undulator cell 37 and moving upstream to cell 21. The resulting dependence is shown in Fig. 4.

For reference, we also computed the expected electron-beam size using the European XFEL lattice model. This model incorporates the actual quadrupole readouts, design

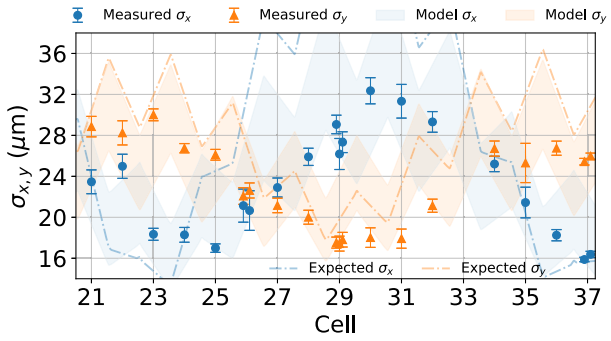

FIG. 4. Measured averaged transverse slice sizes along the SASE1 undulator under mismatched magnetic lattice conditions. The experimental data are shown as blue circles (σ_x) and orange triangles (σ_y). The dashed-dotted line represents the expectation based on an emittance value averaged between the upper and lower bounds, while the shaded regions in the corresponding colors indicate the corrected model within the full emittance range.

Courant-Snyder parameters, and assuming normalized emittance values in the range of $\epsilon_x = 0.37$ to 0.7 mm mrad and $\epsilon_y = 0.46$ to 0.7 mm mrad. The lower estimate is derived from emittance measurements that were conducted at the injector location immediately after our electron beam size measurement shift. The upper estimate, 0.7 mm mrad, is chosen as a conservative boundary.

The expected range of transverse electron-beam sizes is illustrated in Fig. 4 as a dash-dotted line and a shaded area. The dash-dotted line represents an estimate based on the quadrupole readouts during the experiment. To avoid overloading the figure, the assumed emittance was averaged between its upper and lower bounds. To plot the shaded area, which represents the full assumed emittance range, we applied a small correction to the quadrupole current (see Ref. [34]) in our model. This adjustment brings *the model* into closer agreement with the measured data, shown as the shaded area in Fig. 4. The residual amplitude discrepancy of the dash-dotted curve in Fig. 4 likely originates from uncertainties in the upstream beam parameters, whereas the modulation period and node positions match well, confirming that the expected variation is reproduced. This we discuss more extensively in [34].

The experiment presented here is the last in a series of four conducted over the past year. After using a gadolinium oxysulfide scintillator in the first test, we switched to a YAG crystal in the following experiments because of its better spatial resolution. The results were consistent across different conditions, and each time we observed a strong level of correlation. In the final beam time, we managed to take measurements along the SASE1 undulator, which allowed us to collect the full dataset shown in this Letter. This series of experiments confirms that the method gives reproducible results.

In this Letter, we reported the first direct observation of the transversely spiky structure of synchrotron radiation and demonstrated averaged transverse slice size measurements of the electron beam using a simple, noninterferometric setup at the European XFEL. The setup combines a Bragg reflection monochromator with an x-ray imager optimized for synchrotron radiation. An autocorrelation analysis of the measured ensemble enabled retrieval of the second-order correlation function, whose width is related to the transverse size of the electron beam, in accordance with the Van Cittert–Zernike theorem. The method was validated for beam sizes ranging from 16 to 32 μm along the mismatched FODO lattice of the SASE1 undulator, in agreement with beam dynamics predictions. This approach offers a practical diagnostic tool for FELs and other accelerators with comparable beam parameters.

Acknowledgments—We thank Evgeny Saldin for the fruitful discussions, Mikako Makita for assistance with the stuck K-mono motors during one of the shifts, and Serguei Molodtsov for his interest in this work. We thank Giovanni Perosa for his helpful suggestions that improved this article. We thank Winfried Decking for supporting the experimental campaign.

Data availability—The data that support the findings of this article are not publicly available upon publication because it is not technically feasible and/or the cost of preparing, depositing, and hosting the data would be prohibitive within the terms of this research project. The data are available from the authors upon reasonable request.

[1] B. V. Ricketti, E. M. Gauger, and A. Fedrizzi, The coherence time of sunlight in the context of natural and artificial light-harvesting, Sci. Rep. **12**, 5438 (2022).
[2] H. Mashaal, A. Goldstein, D. Feuermann, and J. M. Gordon, First direct measurement of the spatial coherence of sunlight, Opt. Lett. **37**, 3516 (2012).
[3] E. L. Saldin, E. A. Schneidmiller, and M. V. Yurkov, Statistical properties of the radiation from SASE FEL operating in the linear regime, Nucl. Instrum. Methods Phys. Res., Sect. A **407**, 291 (1998).
[4] E. L. Saldin, E. A. Schneidmiller, and M. V. Yurkov, *The Physics of Free Electron Lasers*, Advanced Texts in Physics (Springer, Berlin, Heidelberg, 2000).
[5] R. Bonifacio, L. De Salvo, P. Pierini, N. Piovella, and C. Pellegrini, Spectrum, temporal structure, and fluctuations in a high-gain free-electron laser starting from noise, Phys. Rev. Lett. **73**, 70 (1994).
[6] J. Andruszkow *et al.*, First observation of self-amplified spontaneous emission in a free-electron laser at 109 nm wavelength, Phys. Rev. Lett. **85**, 3825 (2000).
[7] N. Gerasimova, D. La Civita, L. Samoylova, M. Vannoni, R. Villanueva, D. Hickin, R. Carley, R. Gort, B. E. Van Kuiken, P. Miedema, L. Le Guyarder, L. Mercadier, G. Mercurio, J. Schlappa, M. Teichman, A. Yaroslavtsev, H. Sinn, and A. Scherz, The soft x-ray monochromator at the SASE3 beamline of the European XFEL: From design to operation, J. Synchrotron Radiat. **29**, 1299 (2022).

[8] N. Kujala, W. Freund, J. Liu, A. Koch, T. Falk, M. Planas, F. Dietrich, J. Laksman, T. Maltezopoulos, J. Risch, F. Dall'Antonia, and J. Grünert, Hard x-ray single-shot spectrometer at the European x-ray free-electron laser, Rev. Sci. Instrum. **91**, 103101 (2020).

[9] S. Reiche, GENESIS 1.3: A fully 3D time-dependent FEL simulation code, Nucl. Instrum. Methods Phys. Res., Sect. A **429**, 243 (1999).

[10] M. Yabashi, K. Tamasaku, and T. Ishikawa, Characterization of the transverse coherence of hard synchrotron radiation by intensity interferometry, Phys. Rev. Lett. **87**, 140801 (2001).

[11] M. Yabashi, K. Tamasaku, and T. Ishikawa, Measurement of x-ray pulse widths by intensity interferometry, Phys. Rev. Lett. **88**, 244801 (2002).

[12] N. Wiener, Generalized harmonic analysis, Acta Math. **55**, 117 (1930).

[13] A. Khintchine, Korrelationstheorie der stationären stochastischen Prozesse, Math. Ann. **109**, 604 (1934).

[14] J. W. Goodman, *Statistical Optics*, Wiley Classics Library (Wiley, New York, 2000).

[15] J. Goodman, Some effects of target-induced scintillation on optical radar performance, Proc. IEEE **53**, 1688 (1965).

[16] P. H. van Cittert, Die Wahrscheinliche Schwingungsverteilung in Einer von Einer Lichtquelle Direkt Oder Mittels Einer Linse Beleuchteten Ebene, Physica (Amsterdam) **1**, 201 (1934).

[17] F. Zernike, The concept of degree of coherence and its application to optical problems, Physica (Amsterdam) **5**, 785 (1938).

[18] R. H. Brown and R. Q. Twiss, Correlation between photons in two coherent beams of light, Nature (London) **177**, 27 (1956).

[19] R. Hanbury Brown and R. Q. Twiss, A test of a new type of stellar interferometer on sirius, Nature (London) **178**, 1046 (1956).

[20] G. Baym, The physics of Hanbury Brown–Twiss intensity interferometry: from stars to nuclear collisions, arXiv:nucl-th/9804026.

[21] P. Michler, A. Imamoğlu, M. D. Mason, P. J. Carson, G. F. Strouse, and S. K. Buratto, Quantum correlation among photons from a single quantum dot at room temperature, Nature (London) **406**, 968 (2000).

[22] D. Dravins, Intensity interferometry: Optical imaging with kilometer baselines, arXiv:1607.03490.

[23] F. R. Giorgetta, W. C. Swann, L. C. Sinclair, E. Baumann, I. Coddington, and N. R. Newbury, Optical two-way time and frequency transfer over free space, Nat. Photonics **7**, 434 (2013).

[24] A. A. Lutman, Y. Ding, Y. Feng, Z. Huang, M. Messerschmidt, J. Wu, and J. Krzywinski, Femtosecond x-ray free electron laser pulse duration measurement from spectral correlation function, Phys. Rev. ST Accel. Beams **15**, 030705 (2012).

[25] S. Serkez, O. Gorobtsov, D. E. Rivas, M. Meyer, B. Sobko, N. Gerasimova, N. Kujala, and G. Geloni, Wigner distribution of self-amplified spontaneous emission free-electron laser pulses and extracting its autocorrelation, J. Synchrotron Radiat. **28**, 3 (2021).

[26] R. R. Robles, K. A. Larsen, D. Cesar, T. Driver, J. Duris, P. Franz, D. Garratt, V. Guo, G. Just, R. Lemons, M.-F. Lin, R. Obaid, N. Sudar, J. Wang, Z. Zhang, J. Cryan, and A. Marinelli, Spectrotemporal shaping of attosecond x-ray pulses with a fresh-slice free-electron laser, Phys. Rev. Lett. **134**, 115001 (2025).

[27] G. Kube, Review of synchrotron radiation based diagnostics for transverse profile measurements, *Proceedings of DIPAC 2007, Venice, Italy* (2007), https://accelconf.web.cern.ch/d07/papers/moo1a03.pdf.

[28] S. Takano, Beam diagnostics with synchrotron radiation in light sources, *Proceedings of IPAC'10*, Kyoto, Japan (2010), https://proceedings.jacow.org/IPAC10/index.htm.

[29] M. D. Alaimo, M. A. C. Potenza, M. Manfredda, G. Geloni, M. Sztucki, T. Narayanan, and M. Giglio, Probing the transverse coherence of an undulator x-ray beam using Brownian particles, Phys. Rev. Lett. **103**, 194805 (2009).

[30] M. Siano, B. Paroli, M. Potenza, L. Teruzzi, U. Iriso, A. Nosych, E. Solano, L. Torino, D. Butti, A. Goetz, T. Lefevre, S. Mazzoni, and G. Trad, Two-dimensional electron beam size measurements with x-ray heterodyne near field speckles, Phys. Rev. Accel. Beams **25**, 052801 (2022).

[31] M. Labat, O. Chubar, J. Breunlin, N. Hubert, and A. Andersson, Bending magnet synchrotron radiation imaging with large orbital collection angles, Phys. Rev. Lett. **131**, 185001 (2023).

[32] G. Orlandi, P. Heimgartner, R. Ischebeck, C. O. Loch, S. Trovati, P. Valitutti, V. Schlott, M. Ferianis, and G. Penco, Design and experimental tests of free electron laser wire scanners, Phys. Rev. Accel. Beams **19**, 092802 (2016).

[33] T. Lensch, S. Liu, and M. Scholz, The European XFEL wire scanner system, in *Proceedings of the 7th International Beam Instrumentation Conference*, IBIC2018 (JACoW Publishing, Geneva, Switzerland, 2019),10.18429/JACOW-IBIC2018-WEPC05.

[34] Andrei Trebushinin *et al.*, companion paper, Noninterferometric method for transverse electron beam size diagnostic with synchrotron radiation at a free-electron laser, Phys. Rev. ST Accel. Beams **28**, 112801 (2025).

[35] G. Geloni, V. Kocharyan, and E. Saldin, A novel self-seeding scheme for hard x-ray FELs, J. Mod. Opt. **58**, 1391 (2011).

[36] J. Amann *et al.*, Demonstration of self-seeding in a hard-x-ray free-electron laser, Nat. Photonics **6**, 693 (2012).

[37] S. Serkez, Self-seeding XFELs: Operation principle and challenges, Synchrotron Radiat. News **29**, 10 (2016).

[38] C.-K. Min *et al.*, Hard x-ray self-seeding commissioning at PAL-XFEL, J. Synchrotron Radiat. **26**, 1101 (2019).

[39] S. Liu *et al.*, Cascaded hard x-ray self-seeded free-electron laser at megahertz repetition rate, Nat. Photonics **17**, 984 (2023).

[40] J. Wu *et al.*, Hard x-ray self-seeding at LCLS and LCLS-II, Synchrotron Radiat. News **38**, 23 (2025).

[41] S. Liu, G. Geloni, T. Long, W. Qin, V. Kocharyan, J. Yan, L. Cao, N. Kujala, M. Guetg, M. Scholz, and W. Decking, Updates on the hard x-ray self-seeding at the European XFEL, Synchrotron Radiat. News **38**, 11 (2025).

[42] W. Liu, Y. Liu, K. Zhang, T. Liu, and H. Deng, Progress of the hard x-ray self-seeding system at the SHINE, Synchrotron Radiat. News **38**, 30 (2025).

[43] I. Inoue, T. Osaka, T. Hara, H. Tanaka, and M. Yabashi, Reflection self-seeding at SACLA, Synchrotron Radiat. News **38**, 17 (2025).

[44] W. Liu, Y. Liu, K. Zhang, T. Liu, and H. Deng, Progress of the hard X-ray self-seeding system at the SHINE, Synchrotron Radiat. News **38**, 30 (2025).

[45] T. Long, Y. Chen, W. Decking, G. Geloni, M. Guetg, S. Huang, V. Kocharyan, S. Liu, W. Qin, S. Serkez, and J. Yan, Control of bandwidth and signal-to-noise ratio for hard-x-ray self-seeded free-electron lasers, Phys. Rev. Appl. **23**, 044038 (2025).

[46] A. Lutman, F.-J. Decker, J. Arthur, M. Chollet, Y. Feng, J. Hastings, Z. Huang, H. Lemke, H.-D. Nuhn, A. Marinelli, J. Turner, S. Wakatsuki, J. Welch, and D. Zhu, Demonstration of single-crystal self-seeded two-color x-ray free-electron lasers, Phys. Rev. Lett. **113**, 254801 (2014).

[47] A. A. Lutman, T. J. Maxwell, J. P. MacArthur, M. W. Guetg, N. Berrah, R. N. Coffee, Y. Ding, Z. Huang, A. Marinelli, S. Moeller, and J. C. U. Zemella, Fresh-slice multicolour x-ray free-electron lasers, Nat. Photonics **10**, 745 (2016).

[48] G. Geloni, V. Kocharyan, T. Mazza, M. Meyer, E. Saldin, and S. Serkez, Opportunities for two-color Experiments at the SASE3 undulator line of the European XFEL, arXiv:1706.00423.

[49] S. Serkez *et al.*, Opportunities for two-color experiments in the soft x-ray regime at the European XFEL, Appl. Sci. **10**, 2728 (2020).

[50] S. Serkez, Short pulses and 2-color capabilities at the SASE3 FEL line of the European XFEL, (2022), https://accelconf.web.cern.ch/fel2022/pdf/TUAI2_slides.pdf.

[51] J. Duris *et al.*, Tunable isolated attosecond x-ray pulses with gigawatt peak power from a free-electron laser, Nat. Photonics **14**, 30 (2020).

[52] A. Malyzhenkov, Y. P. Arbelo, P. Craievich, P. Dijkstal, E. Ferrari, S. Reiche, T. Schietinger, P. Juranić, and E. Prat, Single- and two-color attosecond hard x-ray free-electron laser pulses with nonlinear compression, Phys. Rev. Res. **2**, 042018(R) (2020).

[53] S. Huang, Y. Ding, Z. Huang, and G. Marcus, Generation of subterawatt-attosecond pulses in a soft x-ray free-electron laser, Phys. Rev. Accel. Beams **19**, 080702 (2016).

[54] E. L. Saldin, E. A. Schneidmiller, and M. V. Yurkov, Self-amplified spontaneous emission FEL with energy-chirped electron beam and its application for generation of attosecond x-ray pulses, Phys. Rev. ST Accel. Beams **9**, 050702 (2006).

[55] Z. Guo *et al.*, Experimental demonstration of attosecond pump–probe spectroscopy with an x-ray free-electron laser, Nat. Photonics **18**, 691 (2024).

[56] P. Franz *et al.*, Terawatt-scale attosecond x-ray pulses from a cascaded superradiant free-electron laser, Nat. Photonics **18**, 698 (2024).

[57] S. Usenko, A. Przystawik, M. A. Jakob, L. L. Lazzarino, G. Brenner, S. Toleikis, C. Haunhorst, D. Kip, and T. Laarmann, Attosecond interferometry with self-amplified spontaneous emission of a free-electron laser, Nat. Commun. **8**, 15626 (2017).

[58] G. Geloni, E. Saldin, E. Schneidmiller, and M. Yurkov, Transverse coherence properties of x-ray beams in third-generation synchrotron radiation sources, Nucl. Instrum. Methods Phys. Res., Sect. A **588**, 463 (2008).

[59] A. Trebushinin, G. Geloni, Y. Rakshun, and S. Serkez, Gaussian random field generator for simulating partially coherent undulator radiation, Optica **9**, 842 (2022).

[60] W. Freund, L. Fröhlich, S. Karabekyan, A. Koch, J. Liu, D. Nölle, J. Wilgen, and J. Grünert, First measurements with the K-monochromator at the European XFEL, J. Synchrotron Radiat. **26**, 1037 (2019).

[61] A. Koch, W. Freund, J. Grünert, M. Planas, T. Roth, L. Samoylova, and V. Lyamayev, Design and initial characterisation of x-ray beam diagnostic imagers for the European XFEL, in *Advances in X-ray Free-Electron Lasers Instrumentation III* (SPIE, 2015), Vol. 9512, pp. 291–302, 10.1117/12.2182463.

[62] N. M. Lockmann, C. Gerth, B. Schmidt, and S. Wesch, Noninvasive THz spectroscopy for bunch current profile reconstructions at MHz repetition rates, Phys. Rev. Accel. Beams **23**, 112801 (2020).

[63] See Supplemental Material at http://link.aps.org/supplemental/10.1103/z89g-f7j6 for an animated version of Fig. 2(a), showing the recorded events.

[64] G. Geloni, E. Saldin, E. Schneidmiller, and M. Yurkov, Statistical Optics approach to the design of beamlines for synchrotron radiation, arXiv:physics/0603269.